


# Birefringent masks that are optimal for generating bottle fields

**Journal Article****Author(s):**

Vella, Anthony; Dourdent, Hippolyte; [Novotny, Lukas](#) ; Alonso, Miguel A.

**Publication date:**

2017-04-17

**Permanent link:**

<https://doi.org/10.3929/ethz-b-000220203>

**Rights / license:**

[In Copyright - Non-Commercial Use Permitted](#)

**Originally published in:**

Optics Express 25(8), <https://doi.org/10.1364/OE.25.009318>

**Funding acknowledgement:**

165841 - Nonlinear optics with hybrid plasmonic-TMDC materials (SNF)

# Birefringent masks that are optimal for generating bottle fields

ANTHONY VELLA<sup>1,2,\*</sup>, HIPPOLYTE DOURDENT<sup>3,4</sup>, LUKAS NOVOTNY<sup>3</sup>,  
AND MIGUEL A. ALONSO<sup>1,2</sup>

<sup>1</sup>The Institute of Optics, University of Rochester, Rochester NY 14627, USA

<sup>2</sup>Center for Coherence and Quantum Optics, University of Rochester, Rochester NY 14627, USA

<sup>3</sup>Photonics Laboratory, ETH Zürich, 8093 Zürich, Switzerland

<sup>4</sup>Institut d'Optique Graduate School, Université Paris-Saclay, 91127 Palaiseau, France

\*avella@optics.rochester.edu

**Abstract:** An optical bottle field containing a three-dimensional intensity null at the focal point can be generated by placing a spatially inhomogeneous birefringent mask at the pupil of an aplanatic high-NA focusing system. We derive the optimal birefringence distribution for which a uniformly polarized input beam is converted into a bottle field with the sharpest possible null in intensity. We show that a stress engineered optical (SEO) window, which has a radially varying retardance, followed by a half-wave plate, performs nearly as well as the optimal solution. Experimental results corroborate that an SEO element can be used to generate a bottle field.

© 2017 Optical Society of America

**OCIS codes:** (050.4865) Optical vortices; (260.6042) Singular optics; (260.5430) Polarization; (260.1440) Birefringence.

## References and links

1. A. Ashkin, J. M. Dziedzic, J. E. Bjorkholm, and S. Chu, "Observation of a single-beam gradient force optical trap for dielectric particles," *Opt. Lett.* **11**, 288–290 (1986).
2. A. Ashkin, "Acceleration and trapping of particles by radiation pressure," *Phys. Rev. Lett.* **24**, 156–159 (1970).
3. A. Ashkin, *History of Optical Trapping and Manipulation of Small Neutral Particles, Atoms, and Molecules* (Springer Berlin Heidelberg, 2001), pp. 1–31.
4. S. Chu, J. E. Bjorkholm, A. Ashkin, and A. Cable, "Experimental observation of optically trapped atoms," *Phys. Rev. Lett.* **57**, 314–317 (1986).
5. A. Ashkin, J. Dziedzic, and T. Yamane, "Optical trapping and manipulation of single cells using infrared laser beams," *Nature* **330**, 769–771 (1987).
6. A. Ashkin and J. Dziedzic, "Optical trapping and manipulation of viruses and bacteria," *Science* **235**, 1517–1521 (1987).
7. A. T. O'Neil and M. J. Padgett, "Axial and lateral trapping efficiency of laguerre–gaussian modes in inverted optical tweezers," *Opt. Comm.* **193**, 45–50 (2001).
8. N. Simpson, D. McGloin, K. Dholakia, L. Allen, and M. Padgett, "Optical tweezers with increased axial trapping efficiency," *J. Mod. Opt.* **45**, 1943–1949 (1998).
9. J. Arlt and M. Padgett, "Generation of a beam with a dark focus surrounded by regions of higher intensity: the optical bottle beam," *Opt. Lett.* **25**, 191–193 (2000).
10. V. G. Shvedov, C. Hnatovsky, A. V. Rode, and W. Krolikowski, "Robust trapping and manipulation of airborne particles with a bottle beam," *Opt. Expr.* **19**, 17350–17356 (2011).
11. S. W. Hell and J. Wichmann, "Breaking the diffraction resolution limit by stimulated emission: stimulated-emission-depletion fluorescence microscopy," *Opt. Lett.* **19**, 780–782 (1994).
12. M. O. Lenz, H. G. Sinclair, A. Savell, J. H. Clegg, A. C. Brown, D. M. Davis, C. Dunsby, M. A. Neil, and P. M. French, "3-d stimulated emission depletion microscopy with programmable aberration correction," *J. Biophotonics* **7**, 29–36 (2014).
13. T. Suyama and Y. Zhang, "3d super-resolution fluorescence microscopy using cylindrical vector beams," *Prog. Electromagn. Res.* **43**, 73–81 (2013).
14. V. G. Shvedov, Y. V. Izdebskaya, A. V. Rode, A. Desyatnikov, W. Krolikowski, and Y. S. Kivshar, "Generation of optical bottle beams by incoherent white-light vortices," *Opt. Express* **16**, 20902–20907 (2008).
15. C.-H. Chen, P.-T. Tai, and W.-F. Hsieh, "Bottle beam from a bare laser for single-beam trapping," *Appl. Opt.* **43**, 6001–6006 (2004).
16. P. Zhang, Z. Zhang, J. Prakash, S. Huang, D. Hernandez, M. Salazar, D. N. Christodoulides, and Z. Chen, "Trapping and transporting aerosols with a single optical bottle beam generated by moiré techniques," *Opt. Lett.* **36**, 1491–1493 (2011).

17. Y. V. Loiko, A. Turpin, T. Kalkandjiev, E. Rafailov, and J. Mompart, "Generating a three-dimensional dark focus from a single conically refracted light beam," *Opt. Lett.* **38**, 4648–4651 (2013).
18. M. Soskin, P. Polyanskii, and O. Arkhlyuk, "Computer-synthesized hologram-based rainbow optical vortices," *New J. Phys.* **6**, 196 (2004).
19. G. Gbur and T. D. Visser, "Coherence vortices in partially coherent beams," *Opt. Comm.* **222**, 117–125 (2003).
20. P. Mahou, N. Curry, D. Pinotsi, G. K. Schierle, and C. Kaminski, "Stimulated emission depletion microscopy to study amyloid fibril formation," *Proc. SPIE* **9931**, 93310U (2015).
21. A. K. Spilman and T. G. Brown, "Stress birefringent, space-variant wave plates for vortex illumination," *Appl. Opt.* **46**, 61–66 (2007).
22. A. M. Beckley, T. G. Brown, and M. A. Alonso, "Full poincaré beams," *Opt. Express* **18**, 10777–10785 (2010).
23. A. M. Beckley, T. G. Brown, and M. A. Alonso, "Full poincaré beams II: partial polarization," *Opt. Express* **20**, 9357–9362 (2012).
24. R. D. Ramkhalawon, T. G. Brown, and M. A. Alonso, "Imaging the polarization of a light field," *Opt. Express* **21**, 4106–4115 (2013).
25. B. G. Zimmerman and T. G. Brown, "Star test image-sampling polarimeter," *Opt. Express* **24**, 23154–23161 (2016).
26. S. Sivankutty, E. R. Andresen, G. Bouwmans, T. G. Brown, M. A. Alonso, and H. Rigneault, "Single-shot polarimetry imaging of multicore fiber," *Opt. Lett.* **41**, 2105–2108 (2016).
27. A. K. Spilman and T. G. Brown, "Stress-induced focal splitting," *Opt. Express* **15**, 8411–8421 (2007).
28. A. Arbabi, Y. Horie, M. Bagheri, and A. Faraon, "Dielectric metasurfaces for complete control of phase and polarization with subwavelength spatial resolution and high transmission," *Nature nanotechnology* (2015).
29. S. Kruk, B. Hopkins, I. I. Kravchenko, A. Miroschnichenko, D. N. Neshev, and Y. S. Kivshar, "Invited article: Broadband highly efficient dielectric metadevices for polarization control," *APL Photonics* **1**, 030801 (2016).
30. B. Richards and E. Wolf, "Electromagnetic diffraction in optical systems. ii. structure of the image field in an aplanatic system," *Proc. R. Soc. London A* **253**, 358–379 (1959).
31. L. Novotny and B. Hecht, *Principles of Nano-Optics* (Cambridge University, 2006), pp. 56–60.
32. M. A. Alonso, "The effect of orbital angular momentum and helicity in the uncertainty-type relations between focal spot size and angular spread," *J. Opt.* **13**, 064016 (2011).
33. K. Y. Bliokh, M. A. Alonso, E. A. Ostrovskaya, and A. Aiello, "Angular momenta and spin-orbit interaction of nonparaxial light in free space," *Phys. Rev. A* **82**, 063825 (2010).
34. L. Marrucci, C. Manzo, and D. Paparo, "Optical spin-to-orbital angular momentum conversion in inhomogeneous anisotropic media," *Phys. Rev. Lett.* **96**, 163905 (2006).
35. F. Cardano, E. Karimi, S. Slussarenko, L. Marrucci, C. de Lisio, and E. Santamato, "Polarization pattern of vector vortex beams generated by q-plates with different topological charges," *Appl. Opt.* **51**, C1–C6 (2012).

## 1. Introduction

Trapping and manipulation of nanoparticles plays a crucial role in biology and physics. The field of laser-based trapping was pioneered by Arthur Ashkin, who developed with co-workers a single-beam gradient-force optical trap, known as "optical tweezers" [1–3]. Nowadays, optical tweezers have found various applications, ranging from cooling and trapping atoms to manipulating live bacteria and viruses [4–6]. The achievement of an efficient trap relies on the optical properties of the particles and the surrounding medium, as well as the physical nature of the light-mediated trapping forces. Optical tweezers are typically implemented using a high numerical aperture (NA) objective, which generates a strong electric field gradient at the focal region. The gradient force created causes particles of higher refractive index than the surrounding medium to be attracted to the light field maximum, and it repels low index particles in a high index environment. Thus, axial trapping efficiency of low index particles can be improved through the use of "hollow" (or "donut") beams, which have intensity minima on the optical propagation axis [7, 8].

In 2000, Arlt and Padgett introduced the concept of an "optical bottle" which represents a beam with a finite axial region of low (ideally null) intensity surrounded in all directions by light [9]. Generating this dark region at the focus creates useful intensity gradients to trap or measure the dynamics of low index particles. For instance, the suitability of an optical bottle beam for particle trapping and manipulation has been confirmed in experiments with atoms and absorbing particles [10]. Optical bottle fields also have applications in stimulated emission depletion (STED) fluorescence microscopy [11], in which the three-dimensional nature of the bottle provides enhanced resolution along the longitudinal direction [12, 13].

Various techniques have been proposed to generate bottle fields [14–17]. Many of these

involve vortices generated by the use of phase masks, spiral phase plates, or spatial light modulators [18, 19]. These methods typically rely on interference between two fundamental Gaussian modes, making them sensitive to alignment errors [20]. Polarization vortex beams have also been generated by propagating a circularly polarized Gaussian beam through a stressed engineered optical (SEO) window [21]. The circular polarization component exiting the stressed window with the opposite handedness acquires a vortex along the axis, so a bottle can be constructed by making sure that the component emerging with the original polarization has an axial null. While SEO elements have been shown to have applications in the generation and detection of spatially varying polarization states [22–26], to date they have not been utilized to generate and optimize a three-dimensional bottle field, although studies on focal splitting [27] have shown fields with an intensity minimum surrounded by high intensity regions.

In this paper, we treat the problem of a general transparent birefringent mask placed in the pupil of an aplanatic high-NA focusing system. We derive the spatial variation of the mask for which a uniformly polarized incident beam is optimally converted into a high-NA bottle field. While such a mask could be fabricated using dielectric metasurfaces [28, 29], we show that the optimal distribution very nearly corresponds to the simple combination of an SEO window followed by a half-wave plate. Preliminary experimental results are presented demonstrating the ability of this practical system to efficiently generate a bottle field without the need for interferometric superposition of different components.

## 2. System layout and notation

Consider the optical system shown in Fig. 1, in which a collimated monochromatic light source with uniform polarization is focused by an aplanatic lens with focal length  $f$  and numerical aperture NA. A thin, transparent birefringent mask (BM) is placed at the back focal (pupil) plane of the system. The radial coordinate in the pupil plane maps onto the focusing angle  $\eta$  after the lens as  $u = \sin \eta$ . The azimuthal pupil coordinate is denoted by  $\phi$ , so that the spatial frequencies over the pupil may be represented using the two-dimensional vector  $\mathbf{u} = (u_x, u_y)$ , which corresponds to the transverse part of the three-dimensional unit direction vector after the lens  $\vec{u} = (u_x, u_y, u_z) = (u \cos \phi, u \sin \phi, (1 - u^2)^{1/2})$ . The lens is assumed to be in air, so that  $u \in [0, \text{NA}]$ . The results presented in later sections can be modified for an immersed imaging system by changing the limits of integration to  $[0, \text{NA}/n]$ , where  $n$  is the refractive index of the immersion medium.

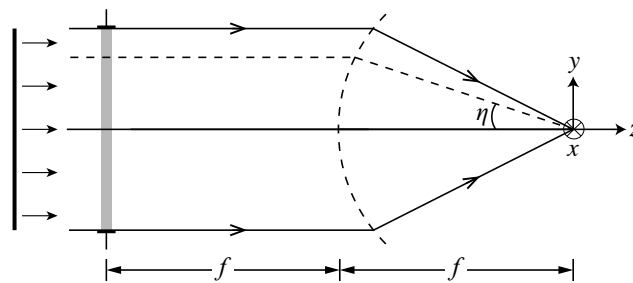


Fig. 1. Schematic of system layout for bottle field generation, in which a thin birefringent mask is placed in the pupil plane of an aplanatic lens. The coordinate in the pupil plane is specified in terms of the focus angle  $\eta$ .

The focusing lens produces a field distribution over the spatial coordinate  $\vec{r} = (x, y, z)$ . For a bottle field, the intensity must vanish at  $\vec{r} = \vec{0}$ , the focal point of the lens. The polarization effect of the lens is assumed to be a rotation of the electric field at each point about the direction of the radial pupil coordinate [30]. The lateral incident field  $\mathbf{E}(\mathbf{u})$  is transformed into a focused

field  $\vec{E}(\vec{r})$  containing both lateral and longitudinal components. The matrix that maps the pupil coordinate to the directional variables after the lens is given by [31]

$$\mathbb{M}_{\text{lens}} = \sqrt{\cos \eta} \begin{bmatrix} \sin^2 \phi + \cos^2 \phi \cos \eta & \sin \phi \cos \phi (\cos \eta - 1) \\ \sin \phi \cos \phi (\cos \eta - 1) & \sin^2 \phi \cos \eta + \cos^2 \phi \\ -\cos \phi \sin \eta & -\sin \phi \sin \eta \end{bmatrix}. \quad (1)$$

### 3. General birefringent mask

The Jones matrix of a general spatially-variant, transparent, thin BM can be written as

$$\mathbb{J}(\mathbf{u}) = \exp[i\Gamma(\mathbf{u})] \{ \exp[i\delta(\mathbf{u})] \mathbf{p}_1(\mathbf{u}) \otimes \mathbf{p}_1^*(\mathbf{u}) + \exp[-i\delta(\mathbf{u})] \mathbf{p}_2(\mathbf{u}) \otimes \mathbf{p}_2^*(\mathbf{u}) \}, \quad (2)$$

where  $\mathbf{p}_{1,2}(\mathbf{u})$  are the two eigenpolarizations at each point of the BM,  $\delta(\mathbf{u})$  is half the phase mismatch between these eigenpolarizations,  $\Gamma(\mathbf{u})$  is a global phase function, and  $\otimes$  indicates an outer product. The fact that the mask is transparent means that this Jones matrix is unitary (that is,  $\Gamma$  and  $\delta$  are real and the eigenpolarizations  $\mathbf{p}_j$  are orthonormal); the fact that the mask is “thin” means that at the pupil plane its effect is local. Up to an arbitrary global phase, the eigenpolarizations of  $\mathbb{J}$  may be written in the form

$$\mathbf{p}_1(\mathbf{u}) = \begin{bmatrix} \cos(\Phi/2) & -\sin(\Phi/2) \\ \sin(\Phi/2) & \cos(\Phi/2) \end{bmatrix} \begin{bmatrix} \cos(\Theta/2) \\ i \sin(\Theta/2) \end{bmatrix}, \quad \mathbf{p}_2(\mathbf{u}) = \begin{bmatrix} 0 & -1 \\ 1 & 0 \end{bmatrix} \cdot \mathbf{p}_1^*(\mathbf{u}), \quad (3)$$

where the functions  $\Theta(\mathbf{u}) \in [-\pi/2, \pi/2]$  and  $\Phi(\mathbf{u}) \in [0, 2\pi]$  are the latitude and longitude angles of  $\mathbf{p}_1(\mathbf{u})$  over the Poincaré sphere. Substituting into Eq. (2), the Jones matrix then becomes

$$\mathbb{J}(\mathbf{u}) = \begin{bmatrix} \cos \delta + i \sin \delta \cos \Theta \cos \Phi & \sin \delta (\sin \Theta + i \cos \Theta \sin \Phi) \\ \sin \delta (-\sin \Theta + i \cos \Theta \sin \Phi) & \cos \delta - i \sin \delta \cos \Theta \cos \Phi \end{bmatrix} \exp(i\Gamma). \quad (4)$$

For the special case of an SEO window with trifold symmetric stress, the retardance depends only on the radial pupil coordinate according to  $\delta(u) = bu$ , where the stress coefficient  $b$  is proportional to the applied force [21, 27]. Because the birefringence results from stress, the eigenpolarizations at all points are linear (thus  $\Theta = 0$ ), and the principal stress direction rotates such that  $\Phi = \phi$ . A half-wave plate can be inserted after the stressed window to reverse the direction of rotation to  $\Phi = -\phi$ .

### 4. Bottle field properties

In Sections 5 through 7 we find the optimal spatial variation of the BM that produces a bottle field with the sharpest possible intensity null. First we must establish the necessary quantities to optimize over, namely: (i) some measure for the width of the bottle, and (ii) the conditions under which the intensity vanishes at the focal point.

#### 4.1. Focused intensity distribution

The focused field is the Fourier transform of the pupil distribution, so the normalized intensity is given by [31]

$$I(\vec{r}) = \frac{1}{(\pi k)^2} \left\| \int A(u) \mathbb{M}_{\text{lens}} \cdot \mathbb{J}(\mathbf{u}) \cdot \mathbf{E}_0 \exp [ik(\vec{u} \cdot \vec{r})] d^2u \right\|^2, \quad (5)$$

where  $k = 2\pi/\lambda$  is the wavenumber,  $A(u)$  is an envelope function accounting for the shape of the incident beam and the aperture (assumed to have rotational symmetry),  $\mathbf{E}_0$  is the polarization of the incident field, and  $\|\vec{v}\|$  denotes the Euclidean norm of a vector  $\vec{v}$ . (Recall that  $\vec{u} \cdot \vec{r} = u_x x + u_y y + u_z z$ .) The normalization factor of  $(\pi k)^{-2}$  in this expression has been chosen for computational convenience. Without loss of generality, we may assume a right circularly polarized input field  $\mathbf{E}_0 = (1, -i)/\sqrt{2}$ , since any other polarization could be converted into this one using a wave plate, whose effect can be absorbed into the BM.

## 4.2. Second derivatives of intensity

To achieve the maximum transverse and longitudinal sharpness of the null in intensity, we must maximize the second derivatives  $I_{x_i x_i}$  evaluated at the origin, which are inversely proportional to the squared widths of the bottle in each dimension  $x_i$ . Starting from Eq. (5), we find that

$$I_{x_i x_i} \Big|_{\vec{r}=\vec{0}} = \frac{2}{\pi^2} \left\| \int A \mathbb{M}_{\text{lens}} \cdot \mathbb{J} \cdot \mathbf{E}_0 u_{x_i} d^2 u \right\|^2. \quad (6)$$

The oscillations of the global phase factor  $\exp(i\Gamma)$  contained within  $\mathbb{J}$  will result in cancellations between the contributions to this integral from different parts of the pupil. Therefore, the second derivatives are as large as possible when  $\Gamma = 0$ . Also, in practice it is difficult to fabricate an element with varying  $\Theta(\mathbf{u})$  since most real-world devices have linear eigenpolarizations. For this reason, we restrict our optimization to birefringent masks with  $\Theta = 0$ . Moreover, we strongly suspect that  $\Theta = 0$  is in fact the optimal solution. Under these simplifications,

$$\mathbb{M}_{\text{lens}} \cdot \mathbb{J} \cdot \mathbf{E}_0 = \sqrt{\cos \eta} \begin{bmatrix} \cos \delta [\cos \eta \cos \phi + i \sin \phi] e^{-i\phi} + i \sin \delta [\cos \eta \cos \phi - i \sin \phi] e^{i(\phi-\Phi)} \\ \cos \delta [\cos \eta \sin \phi - i \cos \phi] e^{-i\phi} + i \sin \delta [\cos \eta \sin \phi + i \cos \phi] e^{i(\phi-\Phi)} \\ -\sin \eta [\cos \delta e^{-i\phi} + i \sin \delta e^{i(\phi-\Phi)}] \end{bmatrix}. \quad (7)$$

In order to avoid a discontinuity at the origin and match the periodic boundary condition on  $\Phi(\mathbf{u})$ , we assume that  $\delta(u)$  only depends on the radial pupil coordinate and that

$$\Phi = m\phi, \quad (8)$$

where  $m$  is an integer. (Note that  $m = -2q$ , where  $q$  is the topological charge of the pattern of eigenpolarization orientations of the mask.) In the paraxial limit, a bottle field can readily be produced for  $m = \pm 1$ . In the nonparaxial case, however, the effects of orbital and spin angular momentum counteract each other only when  $m = -1$  [32, 33]. Otherwise, the bottle becomes filled with light due to constructive interference between the various contributions over the pupil to the longitudinal component of the field. While it is possible to derive conditions guaranteeing a null in intensity for  $m \neq -1$ , these conditions would be difficult to satisfy and would come at the cost of broadening the spatial extent of the focused field. In the derivation that follows we assume that  $\Phi = -\phi$ , and we optimize the remaining function  $\delta(u)$  to produce a bottle field whose minimum in intensity is as narrowly distributed as possible. For a brief discussion of the results obtained for general  $m$ , refer to Appendix A.

Substituting Eqs. (7) and (8) into Eq. (6) and integrating over  $\phi \in [0, 2\pi]$ , the second derivatives of intensity become

$$I_{xx} = I_{yy} = 2 \left\| \int_0^{\text{NA}} A \begin{bmatrix} \frac{1}{2} \xi_{211} \sin \delta \\ \frac{1}{2} \xi_{211} \sin \delta \\ \xi_{310} \cos \delta \end{bmatrix} du \right\|^2, \quad I_{zz} = 2 \left\| \int_0^{\text{NA}} A \begin{bmatrix} \xi_{131} \cos \delta \\ \xi_{131} \cos \delta \\ 0 \end{bmatrix} du \right\|^2, \quad (9)$$

where  $\xi_{nm\ell} = u^n (1 - u^2)^{m/4} (1 + \sqrt{1 - u^2})^\ell$ . Introducing the notation

$$\alpha_{nm\ell, c} = \int_0^{\text{NA}} A \xi_{nm\ell} \cos \delta du, \quad \alpha_{nm\ell, s} = \int_0^{\text{NA}} A \xi_{nm\ell} \sin \delta du, \quad (10)$$

this result may be restated as

$$I_{xx} = I_{yy} = \alpha_{211, s}^2 + 2\alpha_{310, c}^2, \quad (11a)$$

$$I_{zz} = 4\alpha_{131, c}^2. \quad (11b)$$

### 4.3. Bottle beam constraint

The intensity at the focal point can be calculated by substituting Eqs. (7) and (8) into Eq. (5) and integrating over  $\phi$ . This leads to the following requirement for a bottle field:

$$I(\vec{0}) = \frac{1}{k^2} \left\| \int_0^{\text{NA}} A \begin{bmatrix} \xi_{111} \cos \delta \\ \xi_{111} \cos \delta \\ 0 \end{bmatrix} du \right\|^2 = \frac{2}{k^2} \alpha_{111,c}^2 = 0. \quad (12)$$

## 5. Functional form of optimal BM retardance distribution

For the optimization problem one can consider various combinations of  $I_{xx}$ ,  $I_{yy}$ , and  $I_{zz}$  as a measure of the localization of the bottle field. In Sections 6.1 through 6.4 we will propose four different merit functions  $M_1$  through  $M_4$  and solve for the conditions under which each  $M_j$  attains its minimum value. Using the method of Lagrange multipliers, the retardance distribution  $\delta_j(u)$  that minimizes each merit function  $M_j$  is found by solving the system of equations

$$\frac{\partial}{\partial \delta} M_j = \Lambda \frac{\partial}{\partial \delta} \alpha_{111,c}, \quad (13a)$$

$$\alpha_{111,c} = 0, \quad (13b)$$

where the Lagrange multiplier  $\Lambda$  is an arbitrary constant and  $\partial/\partial\delta$  denotes a functional derivative with respect to  $\delta$ . In Section 6, we will find that each optimal solution takes the form

$$\begin{aligned} \delta_j(u) &= \arctan \left( \frac{\xi_{101}}{c_j \xi_{001} + d_j \xi_{200} + e_j \xi_{021}} \right) \\ &= \arctan \left( \frac{u(1 + \sqrt{1 - u^2})}{c_j(1 + \sqrt{1 - u^2}) + d_j u^2 + e_j \sqrt{1 - u^2}(1 + \sqrt{1 - u^2})} \right), \end{aligned} \quad (14)$$

where  $c_j$ ,  $d_j$ , and  $e_j$  are constants. Substituting  $u^2 = [1 + (1 - u^2)^{1/2}][1 - (1 - u^2)^{1/2}]$  in the  $d_j$  term, this simplifies to

$$\delta_j(u) = \arctan \left( \frac{u}{g_j + h_j \sqrt{1 - u^2}} \right), \quad (15)$$

where the new constants  $g_j$  and  $h_j$  are mutually determined by Eqs. (13a) and (13b). The function  $\delta_j(u)$  can be interpreted as the angle traced by the upper half of the elliptic curve  $\{g_j + h_j(1 - u^2)^{1/2}, u\}$  over the interval  $u \in [0, \text{NA}]$ , as illustrated in Fig. 2. In order to avoid singular behavior of the BM at the center of the pupil, we need  $\delta(0) = 0$  and  $\delta'(0) \neq 0$ . The former of these two constraints requires that  $g_j + h_j > 0$ , while the latter is satisfied as long as  $g_j + h_j \neq 0$ . Although the constants  $g_j$  and  $h_j$  depend on  $A(u)$ , the functional form of the optimal solution is invariant to the shape of the input beam and aperture. If  $A(u)$  can be measured experimentally, then the solution can be tailored to compensate for radial nonuniformities in the beam profile.

## 6. Lagrange multiplier constraints for optimal retardance

In this section we evaluate Eq. (13a) for each merit function  $M_j$  and simplify the result to obtain a constraint on the coefficients  $g_j$  and  $h_j$ . In these calculations we make use of the functional derivatives

$$\frac{\partial}{\partial \delta} \alpha_{nml,c} = -A \xi_{nml} \sin \delta, \quad \frac{\partial}{\partial \delta} \alpha_{nml,s} = A \xi_{nml} \cos \delta. \quad (16)$$

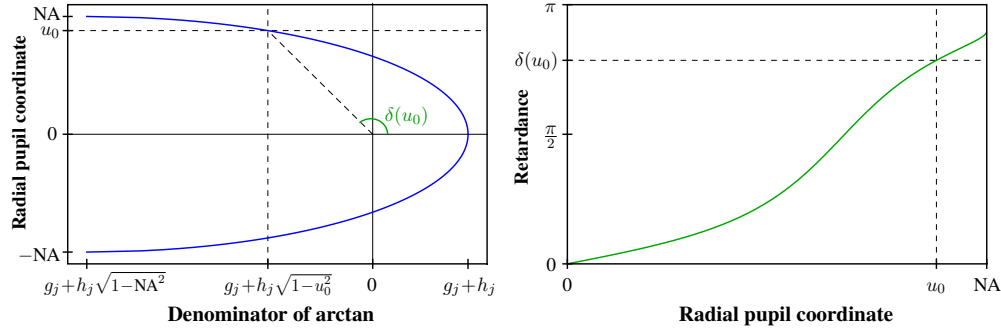


Fig. 2. Illustration of the geometrical meaning of  $\delta_j(u)$ . Dashed lines are drawn to indicate a sample point  $u_0$  on the elliptic curve (left) and the corresponding point on the retardance distribution (right).

### 6.1. Merit function #1: Laplacian of intensity

Let us first minimize the merit function  $M_1 = 1/(I_{xx} + I_{yy} + I_{zz})^{1/2}$ . To simplify the calculation, we solve the equivalent problem of maximizing  $1/M_1^2$ , which is the Laplacian of the intensity at the focal point of the bottle field. Using the Lagrange multiplier method, the condition for optimality is

$$\frac{\partial}{\partial \delta} [I_{xx} + I_{yy} + I_{zz}] = \Lambda \frac{\partial}{\partial \delta} \alpha_{111,c}. \quad (17)$$

Applying the results of the previous sections, this becomes

$$4A [\xi_{211} \alpha_{211,s} \cos \delta - 2(\xi_{310} \alpha_{310,c} + \xi_{131} \alpha_{131,c}) \sin \delta] = -\Lambda A \xi_{111} \alpha_{111,c} \sin \delta. \quad (18)$$

Upon simplification, the solution for  $\delta_1$  takes the form of Eq. (15), subject to the constraints shown in the first row of Table 1.

### 6.2. Merit function #2: characteristic length

We next consider the merit function  $M_2 = (1/I_{xx} + 1/I_{yy} + 1/I_{zz})^{1/2}$ , which represents the length along the diagonal of a box “containing” the bottle. This quantity is referred to as the characteristic length. For the sake of simplicity we minimize  $M_2^2$ , which is equivalent to minimizing  $M_2$ . Substituting into Eq. (13a) and applying the chain rule,

$$-\frac{2 \frac{\partial}{\partial \delta} I_{xx}}{I_{xx}^2} - \frac{\frac{\partial}{\partial \delta} I_{zz}}{I_{zz}^2} = \Lambda \frac{\partial}{\partial \delta} \alpha_{111,c} \quad (19)$$

since  $I_{xx} = I_{yy}$ . Applying the results of the previous sections, this becomes

$$\frac{2 [2\alpha_{211,s} A \xi_{211} \cos \delta - 4\alpha_{310,c} A \xi_{310} \sin \delta]}{(\alpha_{211,s}^2 + 2\alpha_{310,c}^2)^2} - \frac{2\alpha_{131,c} A \xi_{131} \sin \delta}{\alpha_{131,c}^4} = -\Lambda A \xi_{111} \sin \delta. \quad (20)$$

Upon simplification, the solution for  $\delta_2$  takes the form of Eq. (15), subject to the constraints shown in the second row of Table 1.

### 6.3. Merit function #3: volume of bottle

Next we consider the merit function  $M_3 = 1/(I_{xx} I_{yy} I_{zz})^{1/2}$ , which is proportional to the width of the intensity profile in each dimension, thus representing in some sense the “volume” of the



bottle. We will solve the equivalent problem of maximizing  $1/M_3^2$ . Substituting into Eq. (13a), the condition for optimality is

$$2I_{xx}I_{zz} \frac{\partial}{\partial \delta} I_{xx} + I_{xx}^2 \frac{\partial}{\partial \delta} I_{zz} = \Lambda \frac{\partial}{\partial \delta} \alpha_{111,c} \quad (21)$$

since  $I_{xx} = I_{yy}$ . Applying the results of the previous sections, this becomes

$$\alpha_{131,c} (2\alpha_{211,s} A\xi_{211} \cos \delta - 4\alpha_{310,c} A\xi_{310} \sin \delta) - (\alpha_{211,s}^2 + 2\alpha_{310,c}^2) A\xi_{131} \sin \delta = -\Lambda A\xi_{111} \sin \delta, \quad (22)$$

where a factor of  $[8\alpha_{131,c} I_{xx}^2]^{-1}$  has been absorbed into the arbitrary constant  $\Lambda$ . Upon simplification, the solution for  $\delta_3$  takes the form of Eq. (15), subject to the constraints shown in the third row of Table 1.

#### 6.4. Merit function #4: cross-sectional area

Lastly, we consider the merit function  $M_4 = 1/(I_{xx}I_{zz})^{1/2}$ , which is proportional to the cross-sectional area of the bottle in the  $x$ - $z$  plane. In contrast to  $M_3$ , this merit function places equal emphasis on the transverse and longitudinal derivatives. Substitution of  $1/M_4^2$  into Eq. (13a) yields the condition

$$I_{zz} \frac{\partial}{\partial \delta} I_{xx} + I_{xx} \frac{\partial}{\partial \delta} I_{zz} = \Lambda \frac{\partial}{\partial \delta} \alpha_{111,c}. \quad (23)$$

The remainder of the derivation proceeds similarly to the previous case, leading to a solution for  $\delta_4$  of the form of Eq. (15), subject to the constraints shown in the final row of Table 1.

$j$	$M_j$	Constraint 1	Constraint 2
1	$\left[ \frac{1}{I_{xx} + I_{yy} + I_{zz}} \right]^{1/2}$	$\alpha_{111,c} = 0$	$h_1 = \frac{2(\alpha_{131,c} - \alpha_{310,c})}{\alpha_{211,s}}$
2	$\left[ \frac{1}{I_{xx}} + \frac{1}{I_{yy}} + \frac{1}{I_{zz}} \right]^{1/2}$	$\alpha_{111,c} = 0$	$h_2 = \frac{(\alpha_{211,s}^2 + 2\alpha_{310,c}^2)^2}{8\alpha_{211,s}\alpha_{131,c}^3} - \frac{2\alpha_{310,c}}{\alpha_{211,s}}$
3	$\left[ \frac{1}{I_{xx}I_{yy}I_{zz}} \right]^{1/2}$	$\alpha_{111,c} = 0$	$h_3 = \frac{\alpha_{211,s}^2 + 2\alpha_{310,c}^2}{2\alpha_{211,s}\alpha_{131,c}} - \frac{2\alpha_{310,c}}{\alpha_{211,s}}$
4	$\left[ \frac{1}{I_{xx}I_{zz}} \right]^{1/2}$	$\alpha_{111,c} = 0$	$h_4 = \frac{\alpha_{211,s}^2 + 2\alpha_{310,c}^2}{\alpha_{211,s}\alpha_{131,c}} - \frac{2\alpha_{310,c}}{\alpha_{211,s}}$

Table 1. Constraints for optimality of each merit function.

## 7. Numerical solutions

For each merit function, we now have a pair of constraints determining the coefficients  $g_j$  and  $h_j$  that minimize  $M_j$ . The solutions for  $g_j$  and  $h_j$  can be found by numerically solving each set of constraints over a discrete set of NA values. A second solution with identical performance can then be found by flipping the signs of both  $g_j$  and  $h_j$ . With respect to the geometrical interpretation (recall Fig. 2), this amounts to a reflection of the elliptic curve over the vertical axis. To ensure that  $\delta(0) = 0$ , we select the solution for which  $g_j + h_j > 0$ . The results obtained for each merit function are plotted as a function of NA in Fig. 3(a), assuming a uniform envelope

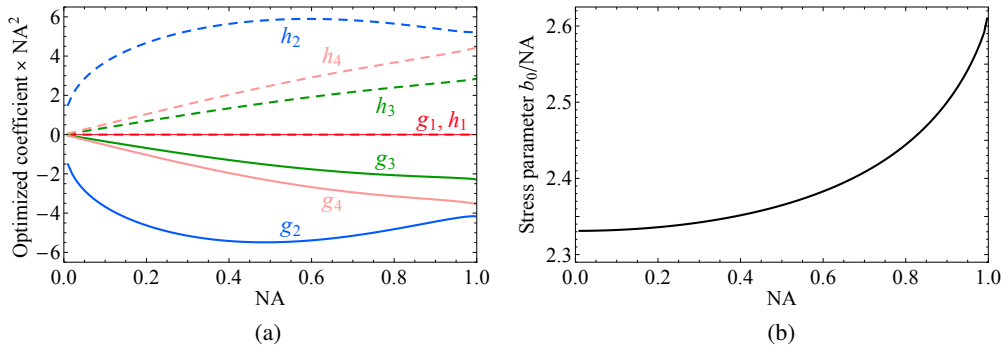


Fig. 3. Numerical solutions for (a) each pair of optimized coefficients  $g_j$  and  $h_j$  and (b) the lowest-order stress parameter  $b_0$  required to produce a bottle field.

function  $A(u) = 1$ . The solutions do not change significantly if  $A(u)$  is instead assumed to be, say, a Gaussian envelope.

For comparison, recall that the retardance distribution of an SEO window is a linear function  $\delta_L(u) = bu$ , and that the azimuthal angle when used in combination with a half-wave plate is  $\Phi = -\phi$ . In this case, the bottle field constraint given in Eq. (12) becomes

$$\int_0^{NA} A(u)u(1-u^2)^{1/4} \left(1 + \sqrt{1-u^2}\right) \cos(bu) du = 0. \quad (24)$$

Since the integrand contains a periodic function, this equation has infinitely many solutions for the stress parameter  $b$ . The smallest solution  $b_0$  is most practical to fabricate (since it requires the least applied force) and produces the best results when used to generate a bottle field. The numerical solution for  $b_0$  (assuming  $A(u) = 1$ ) is plotted as a function of  $NA$  in Fig. 3(b).

The optimized retardance distributions  $\delta_1(u)$  through  $\delta_4(u)$  and the linear solution  $\delta_L(u)$  are plotted in Fig. 4 for six different  $NA$  values. Note that merit function  $M_1$  is minimized by the spatially uniform retardance distribution  $\delta_1(u) = \pi/2$ , which could be produced by a  $q$ -plate with half-wave retardance and topological charge  $q = 1/2$  [34]. As the  $NA$  approaches 1, the other optimized solutions  $\delta_2, \delta_3, \delta_4$  each become increasingly similar to  $\delta_L$ .

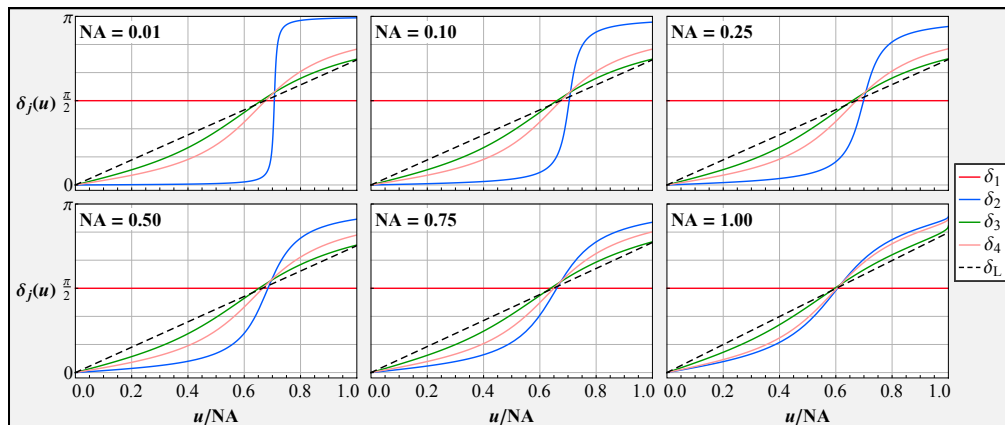


Fig. 4. Comparison of optimized and linear retardance distributions for generating a bottle field, shown for six different  $NA$  values as indicated on the plots. From top to bottom on the right edge of each plot, the curves appear in the following order:  $\delta_2, \delta_4, \delta_3, \delta_L, \delta_1$ .

## 8. Evaluation of numerical solutions

The solutions found in the previous section are now evaluated in terms of the transverse and longitudinal widths of the bottle fields that they produce, which are inversely proportional to the second derivatives of intensity:

$$\sigma_{x_i} \propto \frac{1}{\sqrt{I_{x_i x_i}}}. \quad (25)$$

As shown in Appendix B, for small numerical apertures  $I_{xx} \propto \text{NA}^6$  and  $I_{zz} \propto \text{NA}^8$ . This implies that in the paraxial limit  $\sigma_z \gg \sigma_x$ , as one would expect. The transverse and longitudinal widths of the bottle field (normalized according to their respective NA dependences) are shown in Fig. 5. The ratio  $\sigma_z/\sigma_x$  becomes closer to unity as the NA increases, as seen in Fig. 6. At  $\text{NA} = 1$ , the solution  $\delta_2$  produces the best balance between the widths in each dimension, with  $\sigma_z/\sigma_x = 1.596$ . In comparison, the linear solution produces  $\sigma_z/\sigma_x = 2.616$ . Again, these results assume a uniform envelope function  $A(u) = 1$ . If a Gaussian envelope  $A(u) = \exp(-u^2)$  is used instead, the width of the bottle in each dimension increases by 23% for  $\delta_L$  and by up to 30% for  $\delta_1$  through  $\delta_4$  in the worst-case scenario ( $\text{NA} = 1$ ).

The performance of each solution can be visualized by plotting the cross-section of the theoretical intensity distribution in the  $x$ - $z$  plane. The intensity profiles produced by each retardance distribution are shown in Fig. 7. These plots were simulated under the simplistic assumption that the distribution of the stressed window at the pupil gets directly mapped onto the NA disk, without any aberrations or Fresnel coefficients. Note the slight asymmetry between the upper and lower halves, due to a slight trigonal deviation from rotational symmetry of the intensity profile. In the case of  $\delta_1$ , the uniform retardance distribution simply writes a vortex through spin-orbit interaction, with zero intensity along the entire  $z$ -axis. This shows that a  $q$ -plate

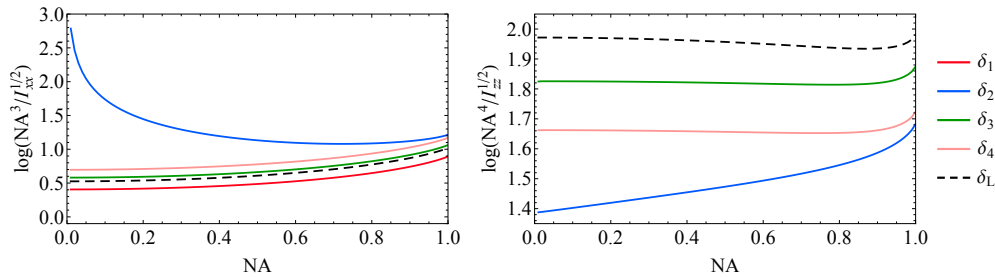


Fig. 5. Logarithm of the transverse (left) and longitudinal (right) widths of the bottle fields generated by each solution, normalized by factors of  $\text{NA}^3$  and  $\text{NA}^4$ , respectively. The longitudinal width of the beam produced by  $\delta_1$  is not shown because it is infinite.

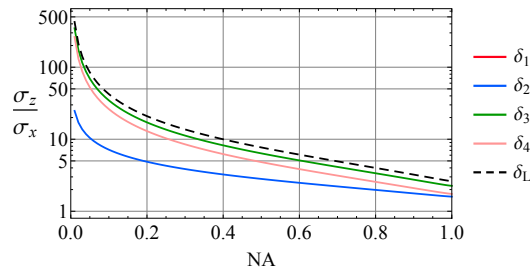


Fig. 6. Ratio of longitudinal to transverse widths of the bottle fields generated by each solution. The ratio for  $\delta_1$  is not shown because it is infinite.

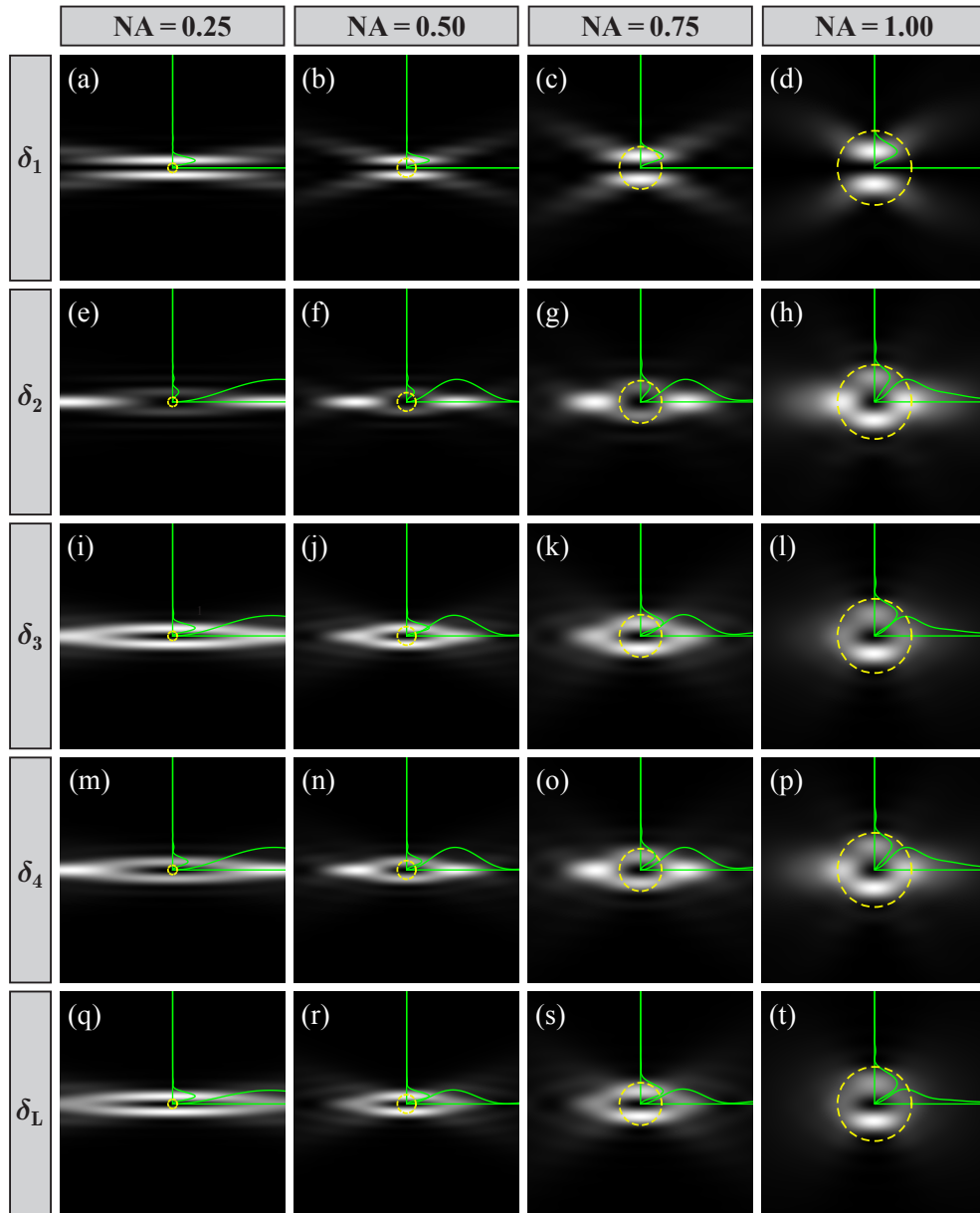


Fig. 7. Simulated cross-sections over the  $x$ - $z$  plane of the focused intensity distributions generated by each solution. The results obtained using the optimized solutions  $\delta_1$  through  $\delta_4$  (a-p) and the linear solution  $\delta_L$  (q-t) are each shown for four different numerical apertures. The solid green curves show the intensity profiles in the  $x$  (vertical) and  $z$  (horizontal) dimensions. The dashed yellow circle is added for scale, with a radius of one wavelength.

with  $\delta = \pi/2$  and  $q = 1/2$ , which has previously been used for vortex beam generation [35], produces the optimal vortex with the sharpest possible null at its center. However, it also implies that merit function  $M_1$  is not really appropriate for qualifying bottle fields since the longitudinal confinement can be sacrificed completely in favor of the transverse one. The remaining solutions  $\delta_2$ ,  $\delta_3$ ,  $\delta_4$ , and  $\delta_L$  all produce bottles with similar appearances, although some subtle differences can be noted. For instance, the intensity lobes along the longitudinal axis are slightly dimmer for  $\delta_L$  than for  $\delta_2$  and  $\delta_4$ . Nevertheless, these results demonstrate that a stressed window can be used to generate a bottle field with nearly optimal sharpness.

## 9. Experimental results

The generation of a bottle field using an SEO window was achieved experimentally using the system shown in Fig. 8. A linear polarizer and quarter-wave plate were used to create a circularly polarized input state. After passing through the SEO and a half-wave plate, the field was focused by a lens with a focal length of 100 mm. An input beam diameter of 3 mm was used, resulting in an effective NA of 0.015. This low numerical aperture was required in order to create a bottle field with a large enough transverse cross-section ( $50 \mu\text{m}$  in diameter) to be resolved by a CMOS camera ( $5 \mu\text{m}$  pixel size). To characterize a high-NA bottle field focus, one could raster-scan a nanoparticle through the laser focus and detect the scattered intensity for every particle position. Similarly, a quantum emitter, such as a quantum dot or a fluorescent molecule, could be raster-scanned and the emitted fluorescence detected. These experiments are in the works and will be published elsewhere. Note that for the low-NA measurement discussed here, it is not necessary to insert a half-wave plate after the stressed window since in the paraxial limit the longitudinal component of the field vanishes at focus for both  $\Phi = \pm\phi$ . For higher numerical apertures, however, the half-wave plate is strictly necessary.

The through focus transverse intensity distribution of the experimental bottle field is shown in Fig. 9. Since the interior width of the bottle is comparable to the pixel size of the sensor, an absolute null could not be measured. However, a local minimum in intensity was observed at focus, with a ratio of 0.43 measured between the intensity at the central pixel and the peak intensity of the surrounding lobes. This demonstrates in principle that the combination of an SEO window and a half-wave plate can be used to generate a bottle field.

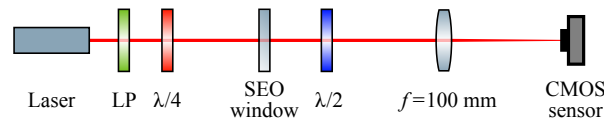


Fig. 8. Schematic of experimental setup for bottle field generation. (LP = linear polarizer,  $\lambda/4$  = quarter-wave plate,  $\lambda/2$  = half-wave plate.)

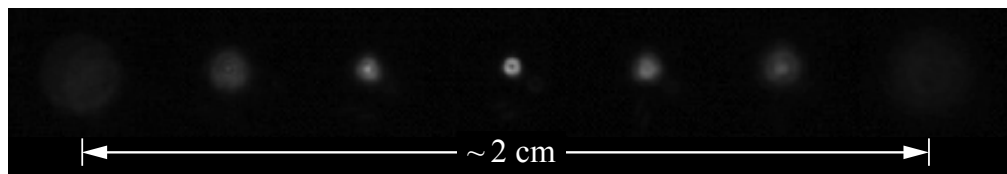


Fig. 9. Evolution through focus of the optical bottle beam's transverse intensity profile over a 2 cm distance along the propagation axis. The intensity distribution at focus has a diameter of  $50 \mu\text{m}$ , matching simulations.

## 10. Concluding remarks

In summary, we have derived the optimal spatial variation of a birefringent mask for generation of a tightly distributed optical bottle field using a high-NA focusing lens. We showed that a practical real-world device, the stress engineered optical element, is theoretically capable of producing a near-optimal bottle field when used in this configuration. The current experimental results verify that an SEO window can be used to generate a focused field with a local minimum of intensity on-axis. However, at low numerical apertures the resulting intensity distribution along the propagation axis has a far greater extent than what is required in optical trapping and microscopy applications. The experimental implementation of a high-NA system comes with the added challenges of compensating for aberrations and angle-dependent polarization effects. If these factors can be accommodated for, the SEO element has the potential to become an efficient and reliable mechanism for bottle field generation that avoids the need of splitting and recombining the input beam.

## Appendix

### A. Results for $m \neq -1$

In Sections 4 through 6 we optimized the retardance distribution of the BM under the assumption that  $\Phi = m\phi$  with  $m = -1$ . Here we reproduce the main results of Section 4 for general  $m$ , an exercise which provides additional insight as to why  $m = -1$  is the optimal choice. We also state the form of the solutions obtained for  $m = 3$ , which are very similar to the  $m = -1$  case.

#### A.1. Second derivatives of intensity

Similarly to Section 4.2, the second derivatives of intensity are obtained by substituting Eqs. (7) and (8) into Eq. (6) and integrating over  $\phi$ . For  $m = 1$ , this leads to

$$I_{xx} = 2 \left\| \int_0^{\text{NA}} A \begin{bmatrix} \xi_{230} \sin \delta \\ \xi_{210} \sin \delta \\ \xi_{310} \cos \delta \end{bmatrix} du \right\|^2, \quad (26a)$$

$$I_{yy} = 2 \left\| \int_0^{\text{NA}} A \begin{bmatrix} \xi_{210} \sin \delta \\ \xi_{230} \sin \delta \\ \xi_{310} \cos \delta \end{bmatrix} du \right\|^2, \quad (26b)$$

$$I_{zz} = 2 \left\| \int_0^{\text{NA}} A \begin{bmatrix} \xi_{131} \cos \delta \\ \xi_{131} \cos \delta \\ 2\xi_{230} \sin \delta \end{bmatrix} du \right\|^2, \quad (26c)$$

where  $\xi_{nm\ell} = u^n(1-u^2)^{m/4}(1+\sqrt{1-u^2})^\ell$  as defined in Section 4.2. For all other integers  $m \neq -1$ ,

$$I_{xx} = I_{yy} = 2 \left\| \int_0^{\text{NA}} A \begin{bmatrix} \frac{1}{2}\Delta_{3m}\bar{\xi}_{211} \sin \delta \\ \frac{1}{2}\Delta_{3m}\bar{\xi}_{211} \sin \delta \\ \xi_{310}[\cos \delta + i(\Delta_{0m} + \Delta_{2m}) \sin \delta] \end{bmatrix} du \right\|^2, \quad (27a)$$

$$I_{zz} = 2 \left\| \int_0^{\text{NA}} A \begin{bmatrix} \xi_{131} \cos \delta - i(\Delta_{2m}\bar{\xi}_{131} - \Delta_{0m}\xi_{131}) \sin \delta \\ \xi_{131} \cos \delta - i(\Delta_{2m}\bar{\xi}_{131} + \Delta_{0m}\xi_{131}) \sin \delta \\ 0 \end{bmatrix} du \right\|^2, \quad (27b)$$

where  $\bar{\xi}_{nm\ell} = u^n(1-u^2)^{m/4}(1-\sqrt{1-u^2})^\ell$  and  $\Delta_{ij}$  is the Kronecker delta, equal to unity when  $i = j$  and zero otherwise. Note that with the exception of the  $m = 1$  and  $m = 3$  cases, the first two vector components contributing to  $I_{xx}$  and  $I_{yy}$  vanish, i.e., the transverse derivatives consist solely of higher-order contributions from the  $z$ -component of the field. This results in a field with a very large spatial extent, which is undesirable. For reasons discussed below, the field is also widely distributed when  $m = 1$ . In the remaining  $m = 3$  case, the second derivatives given in Eq. (27) become

$$I_{xx} = I_{yy} = \bar{\alpha}_{211,s}^2 + \alpha_{310,c}^2, \quad (28a)$$

$$I_{zz} = 4\alpha_{131,c}^2, \quad (28b)$$

where  $\alpha_{nm\ell,c}$  is defined in Eq. (10) and

$$\bar{\alpha}_{nm\ell,s} = \int_0^{\text{NA}} A \bar{\xi}_{nm\ell} \sin \delta \, du. \quad (29)$$

### A.2. Bottle beam constraint

As in Section 4.3, the intensity at the focal point can be calculated by substituting Eqs. (7) and (8) into Eq. (5) and integrating over  $\phi$ . Repeating this process for general  $m$ , we find that for a bottle field

$$I(\vec{0}) = \frac{1}{k^2} \left\| \int_0^{\text{NA}} A \begin{bmatrix} \xi_{111} \cos \delta - i(\Delta_{2m}\bar{\xi}_{111} - \Delta_{0m}\xi_{111}) \sin \delta \\ \xi_{111} \cos \delta - i(\Delta_{2m}\bar{\xi}_{111} + \Delta_{0m}\xi_{111}) \sin \delta \\ 2\Delta_{1m}\xi_{210} \sin \delta \end{bmatrix} du \right\|^2 = 0. \quad (30)$$

For the  $m = 3$  case, this reduces to the condition  $\alpha_{111,c} = 0$ , which is identical to the constraint for  $m = -1$ . For the  $m = 1$  case, an additional constraint  $\alpha_{210,s} = 0$  is necessary to ensure that the longitudinal component of the field vanishes at the focal point. However, this leads to a wider intensity distribution since the transverse derivatives given in Eqs. (26a) and (26b) each contain an  $\alpha_{210,s}$  term. This suggests that among all cases where  $m \neq -1$ , the best performance can be achieved using  $m = 3$ .

### A.3. Functional form of optimal solution and constraints for $m = 3$

The optimization of  $\delta(u)$  for the  $m = 3$  case is very similar to Section 6. The solution obtained for each merit function takes the form

$$\begin{aligned} \delta_j(u) &= \arctan \left( \frac{\bar{\xi}_{101}}{c_j \xi_{001} + d_j \xi_{200} + e_j \xi_{021}} \right) \\ &= \arctan \left( \frac{u(1-\sqrt{1-u^2})}{c_j(1+\sqrt{1-u^2}) + d_j u^2 + e_j \sqrt{1-u^2}(1+\sqrt{1-u^2})} \right), \end{aligned} \quad (31)$$

where the constants  $c_j$ ,  $d_j$ , and  $e_j$  are mutually determined by the constraints shown in Table 2. Note that in this case the transverse second derivatives consist of an integral with numerator  $1 - (1 - u^2)^{1/2}$ , whereas in the  $m = -1$  case the integral depends on  $1 + (1 - u^2)^{1/2}$ . These quantities can be interpreted as the volumes beneath the southern and northern hemispheres, respectively, of a unit sphere sitting on a plane. Therefore, the  $m = -1$  case can be expected to yield larger second derivatives of intensity and consequently the narrowest possible bottle field.

$j$	$M_j$	Constraint 1	Constraint 2	Constraint 3
1	$\left[ \frac{1}{I_{xx} + I_{yy} + I_{zz}} \right]^{1/2}$	$\alpha_{111,c} = 0$	$d_1 = \frac{2\alpha_{310,c}}{\bar{\alpha}_{211,s}}$	$e_1 = \frac{2\alpha_{131,c}}{\bar{\alpha}_{211,s}}$
2	$\left[ \frac{1}{I_{xx}} + \frac{1}{I_{yy}} + \frac{1}{I_{zz}} \right]^{1/2}$	$\alpha_{111,c} = 0$	$d_2 = \frac{2\alpha_{310,c}}{\bar{\alpha}_{211,s}}$	$e_2 = \frac{(\bar{\alpha}_{211,s}^2 + 2\alpha_{310,c}^2)^2}{8\bar{\alpha}_{211,s}\alpha_{131,c}^3}$
3	$\left[ \frac{1}{I_{xx}I_{yy}I_{zz}} \right]^{1/2}$	$\alpha_{111,c} = 0$	$d_3 = \frac{2\alpha_{310,c}}{\bar{\alpha}_{211,s}}$	$e_3 = \frac{\bar{\alpha}_{211,s}^2 + 2\alpha_{310,c}^2}{2\bar{\alpha}_{211,s}\alpha_{131,c}}$
4	$\left[ \frac{1}{I_{xx}I_{zz}} \right]^{1/2}$	$\alpha_{111,c} = 0$	$d_4 = \frac{2\alpha_{310,c}}{\bar{\alpha}_{211,s}}$	$e_4 = \frac{\bar{\alpha}_{211,s}^2 + 2\alpha_{310,c}^2}{\bar{\alpha}_{211,s}\alpha_{131,c}}$

Table 2. Constraints for optimality of each merit function for the  $m = 3$  case.

## B. NA dependence of second derivatives of intensity in the paraxial limit

The Taylor series expansions

$$\xi_{111} = 2u + O(u^3), \quad (32a)$$

$$\xi_{310} = u^3 + O(u^5), \quad (32b)$$

$$\xi_{131} = 2u - 2u^3 + O(u^5), \quad (32c)$$

$$\xi_{211} = 2u^2 + O(u^4) \quad (32d)$$

lead to the paraxial approximations

$$\alpha_{111,c} \approx \int_0^{\text{NA}} 2u \cos \delta du, \quad (33a)$$

$$\alpha_{310,c} \approx \int_0^{\text{NA}} u^3 \cos \delta du, \quad (33b)$$

$$\alpha_{131,c} \approx \int_0^{\text{NA}} (2u - 2u^3) \cos \delta du, \quad (33c)$$

$$\alpha_{211,s} \approx \int_0^{\text{NA}} 2u^2 \sin \delta du. \quad (33d)$$

Since a bottle field is subject to the constraint  $\alpha_{111,c} = 0$ , the first-order component of  $\alpha_{131,c}$  vanishes. Therefore,  $\alpha_{310,c}$  and  $\alpha_{131,c}$  are each proportional to  $\text{NA}^4$ , and  $\alpha_{211,s}$  is proportional to  $\text{NA}^3$ . For  $\text{NA} \ll 1$ , the transverse derivatives given in Eq. (11) are dominated by the  $\text{NA}^6$ -dependent  $\alpha_{211,s}^2$  term, while the longitudinal derivative inherits the  $\text{NA}^8$  dependence of  $\alpha_{131,c}^2$ .

## Funding

National Science Foundation (NSF) (PHY-1507278); Swiss National Science Foundation (SNF) (200020\_165841).

## Acknowledgments

The authors would like to thank Thomas G. Brown for providing the SEO element and for several discussions about birefringence and polarization (and bottle beams in particular) over the years. MAA thanks Pablo Loza for useful discussions. HD and LN thank Xavier Palou for assistance with setting up the experiment.